Int. J. Heat Mass Transfer. Vol. 30, No. 8, pp. 1743–1751, 1987
Printed in Great Britain

0017-9310/87 $3.00+0.00

Wave instability characteristics for the entire regime of mixed convection flow along vertical flat plates

S. L. LEE,† T. S. CHEN and B. F. ARMALY
Department of Mechanical and Aerospace Engineering, University of Missouri–Rolla, Rolla, MO 65401, U.S.A.

(*Received* 8 *August* 1986 *and in final form* 16 *February* 1987)

Abstract—Wave instability of mixed convection flow along an isothermal vertical flat plate is analyzed by the linear theory for the entire mixed convection regime ($0 \leqslant \chi \leqslant 1$, $\chi = [1+(Gr_x/Re_x^2)^{1/4}]^{-1}$) for fluids with Prandtl number of 0.7 and 7. In the analysis, the domain beyond the mainflow boundary layer edge ($\eta \geqslant \eta_\infty$) is solved analytically to provide boundary conditions at $\eta = \eta_\infty$ instead of those at $\eta = \infty$. This treatment is important in the use of the modified Thomas transformation when λ ($\lambda = Re_x^{1/2}+Gr_x^{1/4}$) is small. Dual solutions of critical λ^* values are seen to exist in the range of $0 \leqslant \chi \leqslant 0.5$. The results show that the two limiting neutral stability curves, one for the Blasius flow ($\chi = 1$ or $Gr_x = 0$, with $\lambda^* = 290.6$) and the other for the pure free convection flow ($\chi = 0$ or $Re_x = 0$, with $\lambda^* = 33.33$), correspond to two different modes.

INTRODUCTION

THE PROBLEMS of wave instability for pure forced and pure free convection along isothermal vertical flat plates have been widely investigated. Literature on wave instability of mixed convection flow, however, is somewhat lacking. Mucoglu and Chen [1] solved the wave instability problem of forced-convection-dominated mixed convection flow by employing a fourth-order Runge–Kutta numerical integration scheme along with a filtering technique. From their results, the buoyancy force is found to have a significant effect on the wave instability characteristics of the flow. Recently, Lee *et al.* [2] investigated the flow instability problem of the free-convection-dominated case, with a free stream moving in the direction of the buoyancy force. In the latter study, the main flow quantities were obtained by the local non-similarity method at the second level of truncation. The instability equations were then solved by the modified Thomas transformation method proposed by Lee *et al.* [3]. The results reveal that an increase in the free stream in the direction of the buoyancy force decreases the critical Grashof number. However, the stability curve (i.e. the disturbance frequency vs the Grashof number curve) for an amplification rate of $\alpha_i = -0.005$, where α_i is the imaginary part of the disturbance wave number α, shifts to a higher value of Grashof number. This means that the presence of a free stream that assists the buoyancy force causes instability of the flow to occur at a smaller local Grashof number as compared to the case of pure free convection, but the amplification rate of the disturbances in the downstream locations is reduced significantly. This finding agrees with that of Carey and Gebhart [4] from their study of instability of strongly buoyant mixed convection flow under the boundary condition of uniform surface heat flux.

It is noted that in conventional approaches an analysis of mixed convection flow is divided into two regimes, the forced-convection-dominated regime and the free-convection-dominated regime. The mainflow quantities obtained from solutions of these two regimes may have discrepancies due to numerical errors. Fortunately, a smooth change of the mainflow quantities from the pure forced convection end to the pure free convection end can be achieved by employing a new transformation method such as that proposed by Lee *et al.* [5]. The purpose of the present work is to investigate the linear wave instability of mixed convection flow along an isothermal vertical flat plate for the entire regime by employing the aforementioned smooth change of the mainflow quantities. The disturbance amplitude equations governing the flow are solved by using the modified Thomas method [3]. To ensure highly accurate solutions even at small values of λ ($\lambda = Re_x^{1/2}+Gr_x^{1/4}$), the domain beyond the mainflow boundary layer edge ($\eta \geqslant \eta_\infty$) is solved analytically to provide appropriate boundary conditions at $\eta = \eta_\infty$ for the disturbance amplitude equations.

It should be pointed out that currently no experimental data are available on the wave instability of mixed convection flow. For the pure free convection flow, the existing experimental data [6–8] provide criti-

† Permanent address: Department of Power Mechanical Engineering, National Tsing-Hua University, Hsinchu, Taiwan, Republic of China.

NOMENCLATURE

a_i coefficients of equation (5)
b_i coefficients of equation (6)
f reduced stream function
g gravitational acceleration (9.80665 m s^{-2})
g_j Thomas transformation of the ϕ-function
g_j^* Thomas transformation of the s-function
Gr_x local Grashof number, $g\beta(T_w - T_\infty)X^3/\nu^2$
Gr_δ Grashof number based on δ, $g\beta T_c\delta^3/\nu^2$
m defined as $(X/T_c)(dT_c/dX)$
Pr Prandtl number
Re_x local Reynolds number, $U_\infty X/\nu$
Re_δ Reynolds number based on δ, $U_c\delta/\nu$
s dimensionless amplitude function of the temperature disturbance, $\tilde{s}/T_c$
T temperature [K]
T_c characteristic temperature [K]
u dimensionless streamwise velocity, U/U_c
U streamwise velocity component [m s^{-1}]
U_c characteristic velocity [m s^{-1}]
v dimensionless transverse velocity, $V\lambda/U_c$
V transverse velocity component [m s^{-1}]
X streamwise coordinate measured from the leading edge of the plate [m]
Y transverse coordinate measured normal to the plate [m].

Greek symbols
α dimensionless wave number, $\tilde{\alpha}\delta$
β volumetric coefficient of thermal expansion [K^{-1}] or attenuation coefficient defined by equation (19)
γ attenuation coefficient defined by equation (20)
γ_0 inclination angle of the plate measured from the horizontal position [deg.]
δ characteristic boundary layer thickness, X/λ [m]
η pseudo-similarity coordinate, Y/δ
η_∞ boundary layer edge of the mainflow
θ dimensionless temperature, $(T - T_\infty)/T_c$
λ Re_δ
ξ Gr_δ/Re_δ
ϕ dimensionless amplitude function of the disturbance, $\tilde{\phi}/\delta U_c$
χ modified buoyancy parameter, $[1 + (Gr_x/Re_x^2)^{1/4}]^{-1}$
$\tilde{\psi}$ stream function of the disturbance [m^2 s^{-1}]
ω dimensionless wave frequency, $\tilde{\omega}\delta/U_c$.

Superscript
$\tilde{}$ disturbance quantity.

Subscripts
c characteristic quantity
w condition at the wall
∞ mainflow quantity beyond η_∞.

cal Grashof numbers that do not agree well. Furthermore, the predicted critical Grashof numbers based on the quasi-parallel flow model [2, 9] are two to three orders smaller than the experimental data [6–8]. The wave instability analysis of Blasius flow by the non-parallel flow models [10, 11] has resulted in a lower critical Reynolds number than that predicted by the parallel or quasi-parallel flow model. This is due to the streamwise dependence of the disturbance amplitude function. The non-parallel flow model thus will not necessarily give a better prediction for the pure free convection flow. As a preliminary study to find the instability characteristics of the entire mixed convection regime, the present investigation employs the simpler quasi-parallel flow model [1].

ANALYSIS AND SOLUTION METHOD

In the wave instability problem of a mixed convection flow along an inclined flat plate, the perturbation stream function $\tilde{\psi}$ and perturbation temperature $\tilde{T}$ can assume the respective forms

$$\tilde{\psi}(X, Y, t) = \tilde{\phi}(Y)\exp\left(i\int_{X_0}^{X}\tilde{\alpha}\,dX - i\tilde{\omega}t\right) \quad (1)$$

$$\tilde{T}(X, Y, t) = \tilde{s}(Y)\exp\left(i\int_{X_0}^{X}\tilde{\alpha}\,dX - i\tilde{\omega}t\right) \quad (2)$$

where X_0 denotes an upstream location where natural disturbances occur or artificial disturbances are given. The axial and transverse velocity components of the disturbances are then, respectively

$$\tilde{U} = \partial\tilde{\psi}/\partial Y, \quad \tilde{V} = -\partial\tilde{\psi}/\partial X. \quad (3)$$

Substituting equations (1)–(3) into the linearized disturbance equations (which are based on the linear theory and boundary layer flow approximations, see ref. [12]) and followed by introducing the following dimensionless quantities:

$$u = U/U_c, \quad v = V\lambda/U_c,$$
$$\theta = (T - T_\infty)/T_c, \quad \phi = \tilde{\phi}/\delta U_c,$$
$$s = \tilde{s}/T_c, \quad \alpha = \tilde{\alpha}\delta,$$
$$\omega = \tilde{\omega}\delta/U_c, \quad \lambda = Re_\delta,$$
$$\xi = Gr_\delta/Re_\delta, \quad \Omega = \lambda(\delta/X)(X\,\partial\theta/\partial X + m\theta),$$
$$m = (X/T_c)(dT_c/dX), \quad Re_\delta = U_c\delta/\nu,$$
$$Gr_\delta = \beta g T_c\delta^3/\nu^2, \quad \eta = Y/\delta \quad (4)$$

one obtains

$$\phi^{iv}+a_1\phi'''+a_2\phi''+a_3\phi'+a_4\phi+a_5s'+a_6s=0 \quad (5)$$

$$s''+b_1s'+b_2s+b_3\phi'+b_4\phi=0 \quad (6)$$

$$\phi(0)=\phi'(0)=\phi(\infty)=\phi'(\infty)=0 \quad (7)$$

$$k_1s'(0)+k_2s(0)=s(\infty)=0 \quad (8)$$

and

$$\begin{aligned}
a_1 &= -v\\
a_2 &= -2\alpha^2-i\lambda(\alpha u-\omega)\\
a_3 &= \alpha^2v+v''\\
a_4 &= \alpha^4+i\alpha\lambda(\alpha^2u-\omega\alpha+u'')\\
a_5 &= \xi\sin\gamma_0\\
a_6 &= -i\alpha\xi\cos\gamma_0\\
b_1 &= Pr\,a_1\\
b_2 &= -\alpha^2-i\lambda\,Pr(\alpha u-\omega)\\
b_3 &= -Pr\,\Omega\\
b_4 &= i\alpha\lambda\,Pr\,\theta'
\end{aligned} \quad (9)$$

where the primes denote derivatives with respect to η. The form of boundary condition (8) at $\eta=0$ will be determined according to the appropriate thermal boundary condition. In equations (9), the inclination of the flat plate γ_0 is measured from the horizontal position. It should be pointed out here that the dimensionless transformation as expressed by equation (4) is performed at a certain observation location X. The characteristic velocity $U_c(X)$, characteristic temperature $T_c(X)$, and the characteristic boundary layer thickness $\delta(X)$ are therefore all treated as constants. The wave number α is a complex number ($\alpha=\alpha_r+i\alpha_i$) and the wave frequency ω is a real number.

For the problem of mixed convection flow along an isothermal vertical flat plate (i.e. $\gamma_0=90°$, $T_w=$ constant and $0\leqslant Gr_x/Re_x^2\leqslant\infty$) covering the entire regime from pure forced convection to pure free convection, as considered in this investigation, boundary condition (8) becomes

$$s(0)=s(\infty)=0. \quad (10)$$

The characteristic quantities $U_c(X)$, $T_c(X)$ and $\delta(X)$ and their dependent quantities λ, ξ and m can be conveniently defined, respectively, by

$$\begin{aligned}
&U_c=U_\infty/\chi^2,\quad T_c=T_w-T_\infty,\quad \delta=X/\lambda,\\
&\lambda=Re_x^{1/2}+Gr_x^{1/4},\quad \xi=(1-\chi)^4,\quad m=0
\end{aligned} \quad (11)$$

where $\chi=[1+(Gr_x/Re_x^2)^{1/4}]^{-1}$ is a modified buoyancy parameter which spans between 0 and 1, with $\chi=1$ corresponding to pure forced convection ($Gr_x/Re_x^2=0$) and $\chi=0$ to pure free convection ($Gr_x/Re_x^2=\infty$). It is interesting to note that the value of λ, i.e.

$$\lambda=Re_x^{1/2}+Gr_x^{1/4}=Re_x^{1/2}\chi^{-1}=Gr_x^{1/4}(1-\chi)^{-1} \quad (12)$$

possesses a smooth transition from the pure forced convection end ($\lambda=Re_x^{1/2}$ and $\chi=1$) to the pure free convection end ($\lambda=Gr_x^{1/4}$ and $\chi=0$) as the buoyancy parameter Gr_x/Re_x^2 increases from 0 to ∞. With the definitions of equation (11), the mainflow quantities u, v, u'', v'' and Ω can be expressed as

$$\begin{aligned}
u &= f'\\
v &= (1/4)[(1+\chi)\eta f'-(3-\chi)f+\chi(1-\chi)\,\partial f/\partial\chi]\\
u'' &= f'''\\
v'' &= (1/4)[(1+\chi)\eta f'''-(1-3\chi)f''\\
&\qquad +\chi(1-\chi)\,\partial f''/\partial\chi]\\
\Omega &= -(1/4)[(1+\chi)\eta\theta'+\chi(1-\chi)\,\partial\theta/\partial\chi]
\end{aligned} \quad (13)$$

where the functions f, f', f'', f''', θ and θ' satisfy the following mainflow equations [5]:

$$f'''+[(3-\chi)/4]ff''-[(1-\chi)/2]f'^2+(1-\chi)^4\theta = [\chi(1-\chi)/4](f''\,\partial f/\partial\chi-f'\,\partial f'/\partial\chi) \quad (14)$$

$$\theta''+Pr\,[(3-\chi)/4]f\theta'=Pr\,[\chi(1-\chi)/4]\times(\theta'\,\partial f/\partial\chi-f'\,\partial\theta/\partial\chi) \quad (15)$$

and the associated boundary conditions

$$\begin{aligned}
&f(\chi,0)=f'(\chi,0)=f'(\chi,\infty)-\chi^2=0,\\
&\theta(\chi,0)-1=\theta(\chi,\infty)=0.
\end{aligned} \quad (16)$$

The solution of the mainflow problem, equations (14)–(16), can be found in the paper by Lee *et al.* [5].

Once the mainflow quantities u, u'', v, v'', θ' and Ω are determined by solving the mainflow problem, equations (14)–(16), in the proper domain $0\leqslant\eta\leqslant\eta_\infty$, the stability problem as described by equations (5)–(7) and (10) can be solved by the modified Thomas transformation method [3]. However, in solving the present stability problem the value of λ could be as low as 6, and this fact makes it very difficult to obtain a solution. For instance, at $Pr=7$ and $\chi=0.5$, the critical value of λ is $\lambda^*=6.15$ and the thickness of the stability boundary layer is found to be as large as $\eta=40$, even though the mainflow quantities reach their asymptotic values at $\eta=10$. To remove this numerical difficulty, the domain of the instability problem is divided into two sub-domains $0\leqslant\eta\leqslant\eta_\infty$ and $\eta_\infty\leqslant\eta\leqslant\infty$. In the latter sub-domain $\eta\geqslant\eta_\infty$, all of the mainflow quantities are either constants or zero (i.e. $u=u_\infty=\chi^2$, $v=v_\infty$, $u''=0$, $v''=0$, $\theta'=0$ and $\Omega=0$) and the wave instability equations (5) and (6) become ordinary differential equations with constant coefficients. After solving equations (5) and (6) analytically for the sub-domain $\eta_\infty\leqslant\eta\leqslant\infty$ and imposing the boundary conditions $\phi(\infty)=\phi'(\infty)=s(\infty)=0$, one has (for $\eta\geqslant\eta_\infty$)

$$\phi=C_1e^{-\alpha\eta}+C_2e^{-\beta\eta}+C_3e^{-\gamma\eta} \quad (17)$$

$$s = C_3 e^{-\gamma\eta} \tag{18}$$

where

$$\beta = -v_\infty/2 + [(v_\infty/2)^2 + \alpha^2 + i\lambda(\alpha u_\infty - \omega)]^{1/2} \tag{19}$$

$$\gamma = -Pr\, v_\infty/2 + [(Pr\, v_\infty/2)^2 + \alpha^2 - i\, Pr\, \lambda(\alpha u_\infty - \omega)]^{1/2}. \tag{20}$$

The second and third terms of the ϕ-solution in equation (17) can be neglected only when both the real parts of $(\beta-\alpha)\eta$ and $(\gamma-\alpha)\eta$ are sufficiently large. Under the situation of small λ values, the real parts of $(\beta-\alpha)$ and $(\gamma-\alpha)$ are small. The value of η thus must be increased if one employs this approximation. In the present investigation, for the entire mixed convection flow regime, λ has values in the range of $6 < \lambda < 10^7$. Thus, special care must be exercised in solving the problem. At the edge of the mainflow boundary layer ($\eta = \eta_\infty$), the three parts of the ϕ-solution can be determined from

$$\begin{bmatrix} 1 & 1 & 1 \\ \alpha & \beta & \gamma \\ \alpha^2 & \beta^2 & \gamma^2 \end{bmatrix} \begin{bmatrix} C_1 e^{-\alpha\eta_\infty} \\ C_2 e^{-\beta\eta_\infty} \\ C_3 e^{-\gamma\eta_\infty} \end{bmatrix} = \begin{bmatrix} \phi_n \\ -\phi_n' \\ \phi_n'' \end{bmatrix} \tag{21}$$

$$\begin{bmatrix} C_1 e^{-\alpha\eta_\infty} \\ C_2 e^{-\beta\eta_\infty} \\ C_3 e^{-\gamma\eta_\infty} \end{bmatrix} = \frac{1}{\Delta} \begin{bmatrix} \beta\gamma(\gamma-\beta) & \beta^2-\gamma^2 & \gamma-\beta \\ \alpha\gamma(\alpha-\gamma) & \gamma^2-\alpha^2 & \alpha-\gamma \\ \alpha\beta(\beta-\alpha) & \alpha^2-\beta^2 & \beta-\alpha \end{bmatrix} \begin{bmatrix} \phi_n \\ -\phi_n' \\ \phi_n'' \end{bmatrix} \tag{22}$$

where

$$\Delta = \gamma^2(\beta-\alpha) + \beta^2(\alpha-\gamma) + \alpha^2(\gamma-\beta). \tag{23}$$

In equations (21) and (22), ϕ_n is the value of the amplitude function at $\eta = \eta_n = \eta_\infty$; i.e. $\phi_n = \phi(\eta_n) = \phi(\eta_\infty)$. Note here that η_∞ denotes the edge of the mainflow boundary layer and η_n is defined by $\eta_j = (j-1)h$, with h being the step size. At $\eta = \eta_{n+1}$ and $\eta = \eta_{n+2}$

$$\begin{bmatrix} \phi_{n+1} \\ \phi_{n+1}'' \\ \phi_{n+2} \\ \phi_{n+2}'' \end{bmatrix} = \begin{bmatrix} Z_1 & Z_2 & Z_3 \\ \alpha^2 Z_1 & \beta^2 Z_2 & \gamma^2 Z_3 \\ Z_1^2 & Z_2^2 & Z_3^2 \\ \alpha^2 Z_1^2 & \beta^2 Z_2^2 & \gamma^2 Z_3^2 \end{bmatrix} \begin{bmatrix} C_1 e^{-\alpha\eta_\infty} \\ C_2 e^{-\beta\eta_\infty} \\ C_3 e^{-\gamma\eta_\infty} \end{bmatrix} \tag{24}$$

where

$$Z_1 = \exp(-\alpha h), \quad Z_2 = \exp(-\beta h), \quad Z_3 = \exp(-\gamma h). \tag{25}$$

Substituting equation (22) into equation (24) and expanding the various ϕ-functions on both sides of the resulting equation by the standard Thomas transformation [13], one arrives at four algebraic equations in the form

$$[A][g_{n+1}, g_{n+2}, g_{n+3}, g_{n+4}]^T = [B][g_{n-2}, g_{n-1}, g_n]^T. \tag{26}$$

In equation (26), g_j is the Thomas transformation of the ϕ-function and its derivatives, $[A]$ is a 4 by 4 matrix, and $[B]$ is a 4 by 3 matrix. Equation (26) is then solved to obtain the expressions for g_{n+1} and g_{n+2} in terms of g_{n-2}, g_{n-1} and g_n. For the temperature amplitude function, as in ref. [3] equation (18) implies

$$g_{n+1}^* = Z_3 g_n^*, \quad g_{n+2}^* = Z_3^2 g_n^*, \tag{27}$$

with g_j^* denoting the Thomas transformation of the s-function and its derivatives. Equations (26) and (27) are then used as the boundary conditions at $\eta = \eta_\infty$.

RESULTS AND DISCUSSION

Neutral stability curves and critical stability results were obtained for $Pr = 0.7$ and 7. They cover the entire mixed convection flow regime ($0 \leqslant Gr_x/Re_x^2 \leqslant \infty$ or $1 \geqslant \chi \geqslant 0$). In the numerical calculations, the eigenvalue problem involved finding α_r and α_i for given ω and λ under fixed Pr and χ for the mainflow. Müller's method [14] was employed to find the eigenvalue $\alpha = \alpha_r + i\alpha_i$ until convergence of a solution was attained. In mapping out a neutral stability curve, the value of ω or λ was adjusted by Müller's method until the solution was converged and at the same time $\alpha_i = 0$ was satisfied within a certain tolerance.

Figure 1 shows the neutral stability curves for $Pr = 0.7$ in the ω vs λ plane for $\chi = 0$, 0.15, 0.35 and 0.5. The curve for $\chi = 0$ corresponds to pure free convection. Calculations were proceeded from $\chi = 0$ to 0.15 and so on. It should be noted that the curve for $\chi = 0.5$ is incomplete and no solution can be obtained for $\chi > 0.5$. In fact, the eigenvalue $\alpha(=\alpha_r + i\alpha_i)$ for given ω and λ becomes increasingly difficult to obtain as χ becomes larger. As an illustration, the equi-potential curves of $|\phi(0)|$ in the α-plane is mapped out in Fig. 2 for $\chi = 0.35$ and $(\omega, \lambda) = (0.03112, 47.79)$. In the region $0 \leqslant \alpha_r \leqslant 0.3$ and $-0.1 \leqslant \alpha_i \leqslant 0.21$, there are at least seven eigenvalues that satisfy $\phi(0) = 0$. Among them, the eigenvalue with $\alpha_r = 0.1205$ and $\alpha_i = 0$ possesses the minimum value of α_i. The neutral stability curve thus is based on this particular eigenvalue, because it corresponds to the least stable mode of disturbances. To reach this eigenvalue, an initial guess must fall inside the closed curve labeled with $100|\phi(0)| = 90$ which encloses this particular eigenvalue. The allowable initial guess for α_r and α_i should lie within $\Delta\alpha_r = \Delta\alpha_i = \pm 0.01$. Unfortunately, the closed region keeps shrinking as χ increases, especially on the upper branch of the neutral stability curve. The eigenvalues eventually disappear from the upper branch of the

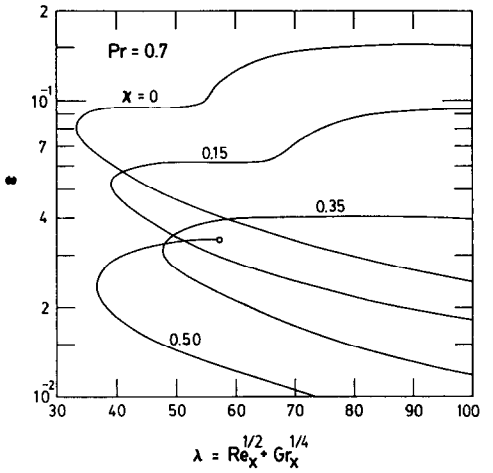

FIG. 1. Neutral stability curves based on Mode I for $Pr = 0.7$.

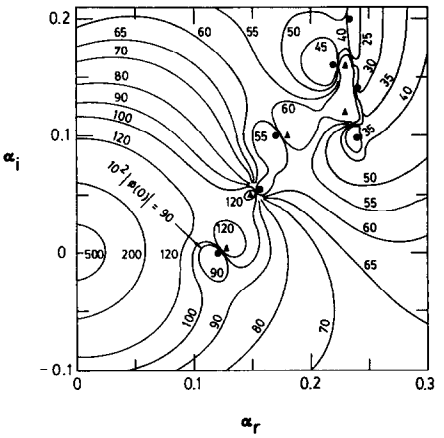

FIG. 2. Equi-potential curves of $|\phi(0)|$ in the α-plane for $Pr = 0.7$, $\chi = 0.35$ and $(\omega, \lambda) = (0.03112, 47.79)$. The solid dots denote the eigenvalues and the solid triangles denote the local maximums.

neutral stability curve for $\chi = 0.5$ and $\lambda > 57$. A similar behavior was found for $Pr = 7$, but to conserve space the neutral stability curves for $Pr = 7$ are not shown.

Because calculations could not be accomplished from $\chi = 0$ to 1, another effort was undertaken to go from $\chi = 1$ (the pure forced convection end) to $\chi = 0$ (the pure free convection end). Starting with the neutral stability results for the Blasius flow (i.e. $\chi = 1$, $\omega^* = 0.07098$ and $\lambda^* = 290.6$, with the superscript '*' denoting quantities at the critical point), one can accomplish the mapping of neutral stability curves from $\chi = 1$ to 0 without any particular difficulty (note that solution by the Runge–Kutta method will fail when $\lambda > 10^4$, see ref. [3]). Unexpectedly, dual solutions were found to exist for $0 \leqslant \chi \leqslant 0.5$. That is, the solutions for $0 \leqslant \chi \leqslant 0.5$ as χ proceeds from 1 to 0 are different from those as χ proceeds from 0 to 0.5. For instance, for $Pr = 0.7$ and $\chi = 0.35$, a neutral stability curve other than the one shown in Fig. 1 is obtained. For convenience, the former (having the critical values $\omega_1^* = 0.03112$ and $\lambda_1^* = 47.79$) will be

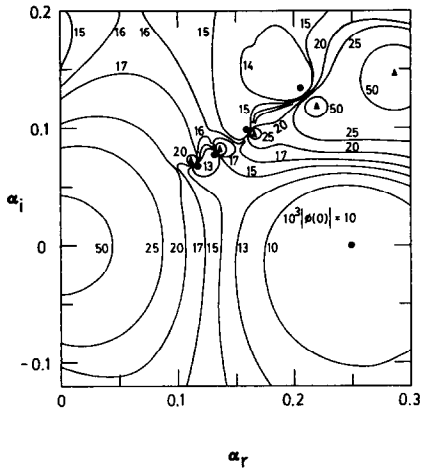

FIG. 3. Equi-potential curves of $|\phi(0)|$ in the α-plane for $Pr = 0.7$, $\chi = 0.35$ and $(\omega, \lambda) = (0.01335, 5.460 \times 10^4)$.

designated as Mode I and the latter (having the critical values $\omega_2^* = 0.01335$ and $\lambda_2^* = 5.460 \times 10^4$) as Mode II. It is important to note that following a smooth path in the ω vs λ plane from $(\omega_1^*, \lambda_1^*)$ on Mode I to $(\omega_2^*, \lambda_2^*)$ on Mode II, one will see a continuous transition of the equi-potential map of $|\phi(0)|$ from the one shown in Fig. 2 to that shown in Fig. 3. All of the seven eigenvalues in Fig. 2 disappear as the change from Mode I to Mode II takes place. New closed regions containing eigenvalues generate, grow and decay later. One of them, however, grows to a very large size and contains the eigenvalue with $\alpha_r = 0.2493$ and $\alpha_i = 0$ which has the minimum value of α_i (see Fig. 3). Therefore, the family of eigenvalues for Mode I is different from that for Mode II.

The neutral stability curves for $Pr = 0.7$ based on Mode II are plotted in Figs. 4 and 5. From Fig. 4, one can see that the neutral stability curve shifts to higher λ values very rapidly as χ decreases from 1 to 0.5. A change in the shape of the neutral stability curve occurs as χ decreases further to 0.3. The detailed changing of the neutral stability curve from $\chi = 0.5$. to 0.3 is shown in Fig. 5. As χ decreases from 0.5 to 0.35, a 'neck' is seen to form on the tip of the curve. It is rather interesting to see that the neutral stability curve is separated into two regions at $\chi = 0.325$. Two critical points thus can be identified as shown in Fig. 5, with one being labeled with H (head) and the other with S (shoulder). The two-region neutral stability curve exists at least in the χ range of $0.0323 \leqslant \chi \leqslant 0.0326$. The head region, however, was not found for $\chi \leqslant 0.32$. Based on the shoulder region, the neutral stability curve moves to smaller λ values as χ decreases from 0.3 to 0 (see Fig. 4). A similar behavior was found to exist for $Pr = 7$. However, the neutral stability curves for $Pr = 7$ are not illustrated in this paper.

The critical values of λ^* for $Pr = 0.7$ and 7 are plotted in Fig. 6 as a function of χ. These values are listed in Table 1 for $Pr = 0.7$ and in Table 2 for $Pr = 7$.

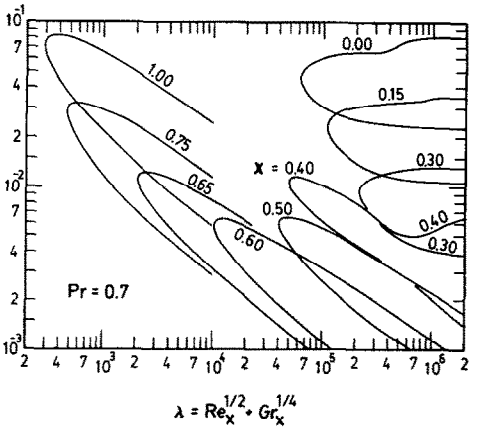

FIG. 4. Neutral stability curves based on Mode II for $0 \leqslant \chi \leqslant 1$, $Pr = 0.7$.

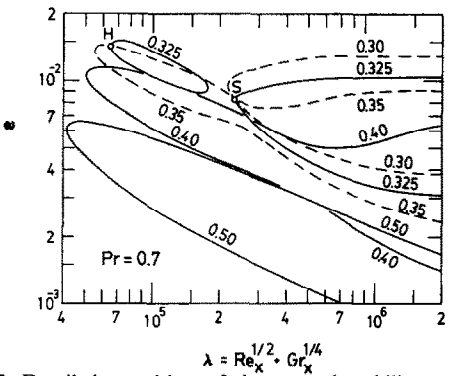

FIG. 5. Detailed transition of the neutral stability curves from $\chi = 0.5$ to 0.3 based on Mode II for $Pr = 0.7$.

The results corresponding to Mode I are shown in the left lower portion of Fig. 6. As discussed earlier, the eigenvalues for this mode vanish when $\chi \geqslant 0.5$. The results by Lee *et al.* [2] are also plotted in the figure for comparison. In their investigation, Lee *et al.* [2] employed the local non-similarity method in solving the transformed mainflow equations and the modified Thomas method [3] in solving the flow instability problem. Very good agreement is seen between the present results and those of Lee *et al.* [2], particularly for $Pr = 0.7$. The results in Fig. 6 are presented in terms of

$$\lambda^* = (Re_x^{1/2} + Gr_x^{1/4})^* = (Gr_x^{1/4})^*(1-\chi)^{-1}.$$

If they were plotted in terms of $(Gr_x^{1/4})^* = \lambda^*(1-\chi)$, one would see that the critical Grashof number $(Gr_x^{1/4})^*$ would decrease monotonously as χ increases. This behavior agrees with the results of Carey and Gebhart [4] for the case of uniform surface heat flux (see the discussion in Lee *et al.* [2]).

The curves on the upper portion of Fig. 6 are the results based on Mode II. A sharp increase in λ^* can be observed near $\chi = 0.6$ as χ decreases from 1 to 0.5. In addition, a crossover of the curves for $Pr = 0.7$ and 7 can be seen at $\chi = 0.614$. This means that the buoyancy flow has strong positive effects on the flow stability for both $Pr = 0.7$ and 7. The effects are

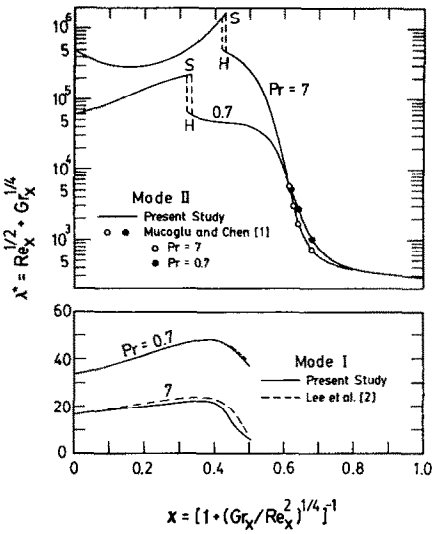

FIG. 6. Critical λ^* values as a function of χ ($0 \leqslant \chi \leqslant 1$) for $Pr = 0.7$ and 7.

stronger for $Pr = 0.7$ than for $Pr = 7$ when $\chi > 0.614$ and vice versa when $\chi < 0.614$. The results from Mucoglu and Chen [1] are seen to be in excellent agreement with the present investigation. A jump of the λ^* values is found in a small range of χ values near $\chi = 0.325$ for $Pr = 0.7$ and near $\chi = 0.425$ for $Pr = 7$ where two-region neutral stability curves exist. As pointed out earlier, the letter 'H' denotes the critical point based on the 'head' region and 'S' denotes that based on the 'shoulder' region. One can also see that dual solutions exist in the range of $0 \leqslant \chi \leqslant 0.5$ with λ^* values being of the order of 10 for Mode I and of the order of 10^5 for Mode II. Hence, in the range of $0 \leqslant \chi \leqslant 0.5$ Mode II is not important as far as instability of the flow is concerned. The mechanism of how the critical value λ^* in a physical flow changes from Mode I to Mode II in the vicinity of $\chi = 0.5$ is not known. This is not due to the use of the quasi-parallel flow model in the present analysis, because the change between Mode I and Mode II is from $O(10)$ to $O(10^5)$ and the error from the quasi-parallel flow model is expected to be only a few percent (see refs. [10, 11]). Unfortunately, this paper is the only investigation that examines the flow instability for the entire mixed convection regime and there are no experimental data available for comparison to substantiate the present predictions.

For the pure forced convection case ($\chi = 1$), the prediction agrees well with available experimental data. As compared with the experimental value of $\lambda^* = 220$ from Schubauer and Skramstad [15] and Ross *et al.* [16], the quasi-parallel flow model predicts a critical Reynolds number of $\lambda^* = 290.6$ [3], an over-prediction of about 32%. This discrepancy can be reduced when the effect of the axial variation of the disturbance amplitude function is taken into account in the analysis by the non-parallel flow model (see refs. [10, 11]). For the pure free convection case ($\chi = 0$), however, the available experimental data have wide

Table 1. The critical stability results for $Pr = 0.7$

χ	Gr_x/Re_x^2	Mode I λ^*	Mode I ω^*	Mode I α_r^*	Mode II λ^*	Mode II ω^*	Mode II α_r^*
0.00	∞	33.33	0.08174	0.1634	6.201 (4)	0.04595	0.4384
0.05	1.303 (+5)	35.07	0.07039	0.1558	7.300 (4)	0.03709	0.4059
0.10	6.561 (+3)	36.97	0.06046	0.1482	8.862 (4)	0.02950	0.3732
0.15	1.031 (+3)	39.05	0.05201	0.1412	1.106 (5)	0.02303	0.3398
0.20	2.560 (+2)	41.30	0.04492	0.1348	1.400 (5)	0.01762	0.3051
0.25	8.100 (+1)	43.66	0.03908	0.1291	1.744 (5)	0.01332	0.2685
0.30	2.964 (+1)	45.97	0.03452	0.1245	2.155 (5)	0.00964	0.2284
0.325	1.861 (+1)	46.98	0.03263	0.1222	(S) 2.254 (5)	0.00838	0.2100
					(H) 6.246 (4)	0.01453	0.2666
0.35	1.190 (+1)	47.79	0.03112	0.1205	5.460 (4)	0.01335	0.2493
0.40	5.063 (+0)	48.00	0.02864	0.1157	4.851 (4)	0.01102	0.2145
0.45	2.232 (+0)	44.04	0.02646	0.1060	4.544 (4)	0.00828	0.1658
0.50	1.000 (+0)	36.63	0.02334	0.0864	4.102 (4)	0.00601	0.1169
0.55	4.481 (−1)	—	—	—	2.829 (4)	0.00481	0.0812
0.60	1.975 (−1)	—	—	—	1.012 (4)	0.00582	0.0709
0.65	8.407 (−2)	—	—	—	2.070 (3)	0.01129	0.0871
0.75	1.235 (−2)	—	—	—	4.724 (2)	0.02822	0.1285
1.00	0	—	—	—	2.906 (2)	0.07098	0.1764

$a(b) = a \times 10^b$.
(S) = shoulder.
(H) = head.

Table 2. The critical stability results for $Pr = 7$

χ	Gr_x/Re_x^2	Mode I λ^*	Mode I ω^*	Mode I α_r^*	Mode II λ^*	Mode II ω^*	Mode II α_r^*
0.00	∞	16.82	0.11436	0.3813	4.927 (5)	0.04092	0.6705
0.05	1.303 (+5)	17.68	0.09842	0.3631	3.804 (5)	0.03127	0.6001
0.10	6.561 (+3)	18.56	0.08458	0.3456	3.054 (5)	0.02536	0.5595
0.15	1.031 (+3)	19.43	0.07277	0.3293	2.884 (5)	0.02055	0.5204
0.20	2.560 (+2)	20.25	0.06290	0.3143	3.013 (5)	0.01522	0.4521
0.25	8.100 (+1)	20.98	0.05476	0.2999	3.446 (5)	0.01112	0.3857
0.30	2.964 (+1)	21.60	0.04801	0.2836	4.357 (5)	0.00771	0.3118
0.35	1.190 (+1)	22.09	0.04170	0.2570	6.265 (5)	0.00482	0.2262
0.40	5.063 (+0)	21.33	0.03318	0.1985	1.094 (6)	0.00249	0.1342
0.425	3.351 (+0)	18.99	0.02633	0.1475	(S) 1.644 (6)	0.00164	0.0882
					(H) 4.835 (5)	0.00249	0.1150
0.45	2.232 (+0)	12.44	0.01726	0.0860	4.157 (5)	0.00213	0.0897
0.50	1.000 (+0)	6.15	0.01301	0.0534	2.550 (5)	0.00167	0.0568
0.55	4.481 (−1)	—	—	—	1.088 (5)	0.00168	0.0413
0.60	1.975 (−1)	—	—	—	1.540 (4)	0.00352	0.0482
0.65	8.407 (−2)	—	—	—	1.270 (3)	0.01071	0.0766
0.75	1.235 (−2)	—	—	—	4.318 (2)	0.02885	0.1293
1.00	0	—	—	—	2.906 (2)	0.07098	0.1764

$a(b) = a \times 10^b$.
(S) = shoulder.
(H) = head.

Table 3. A comparison of critical Grashof numbers for pure free convection

Investigator	Year	Fluid	$(Gr_x^{1/4})^*$
Tritton [6]	1963	air	55.5
Lock *et al.* [7]	1967	air	164
Lloyd and Sparrow [8]	1970	water	111
Present predictions		$Pr = 0.7$	33.33
(Mode I)		$Pr = 7$	16.82

scatters among investigators. The experimental data along with the present predictions (based on Mode I) are listed in Table 3 for comparisons. It is interesting to note that the value of $(Gr_x^{1/4})^*$ obtained by Tritton [6] for air is about 50% lower than that obtained by Lloyd and Sparrow [8] for water. In contrast, Lock *et al.* [7] obtained a value of $(Gr_x^{1/4})^*$ for air which is about 50% higher than the value of Lloyd and Sparrow [8]. The present investigation predicts a value of $(Gr_x^{1/4})^*$ for air ($Pr = 0.7$) which is about twice as large as for water ($Pr = 7$). More experiments and analyses are needed to examine the instability characteristics of pure free convection and strongly buoyant mixed convection flows and to resolve the great discrepancies that exist between results from analyses and measurements.

CONCLUSION

Wave instability of mixed convection flow along isothermal flat plates is investigated by the linear quasi-parallel flow model for the entire regime. The flow instability equations for the disturbance amplitude functions are solved by employing a modified Thomas method. Dual solutions (Mode I and Mode II) are found to exist in the range of $0 \leqslant \chi \leqslant 0.5$ for both $Pr = 0.7$ and 7. The two neutral stability curves, one for the Blasius flow ($\chi = 1$ and $\lambda^* = 290.6$) and the other for the pure free convection flow ($\chi = 0$ and $\lambda^* = 33.33$), are found to originate from two different modes, because the family of eigenvalues based on Mode I is different from that based on Mode II.

Acknowledgement—The work reported in this paper was supported in part by grants from the National Science Foundation (NSF MEA 83-00785) and the University of Missouri (Weldon Spring-Chen 85-86).

REFERENCES

1. A. Mucoglu and T. S. Chen, Wave instability of mixed convection flow along a vertical flat plate, *Numer. Heat Transfer* **1,** 267–283 (1978).
2. S. L. Lee, T. S. Chen and B. F. Armaly, Free stream effects on the wave instability of buoyant flows along an isothermal vertical flat plate, *Int. J. Heat Mass Transfer* **30,** 1556–1558 (1987).
3. S. L. Lee, T. S. Chen and B. F. Armaly, New finite difference solution methods for wave instability problems, *Numer. Heat Transfer* **10,** 1–18 (1986).
4. V. P. Carey and B. Gebhart, The stability and disturbance-amplification characteristics of vertical mixed convection flow, *J. Fluid Mech.* **127,** 185–201 (1983).
5. S. L. Lee, T. S. Chen and B. F. Armaly, Mixed convection along isothermal vertical cylinders and needles, *Proc. Eighth Int. Heat Transfer Conf.*, Vol. 3, pp. 1425–1432 (1986).
6. D. J. Tritton, Transition to turbulence in the free convection boundary layers on an inclined heated plate, *J. Fluid Mech.* **16,** 417–435 (1963).
7. G. S. H. Lock, C. Gort and G. R. Pond, A study of instability in free convection from an inclined plate, *Appl. Scient. Res.* **18,** 171–182 (1967).
8. J. R. Lloyd and E. M. Sparrow, On the instability of natural convection flow on inclined plates, *J. Fluid Mech.* **42,** 465–470 (1970).
9. K. L. Tzuoo, T. S. Chen and B. F. Armaly, Wave instability of natural convection flow on inclined surfaces, *ASME J. Heat Transfer* **107,** 107–111 (1985).
10. M. Bouthier, Stabilité linéaire des écoulements presque parallèles. Partie II. La couche limite de Blasius, *J. Méc.* **12,** 75–95 (1973).
11. M. Gaster, On the effects of boundary-layer growth on flow stability, *J. Fluid Mech.* **66,** 465–480 (1974).
12. T. S. Chen and A. Moutsoglu, Wave instability of mixed convection flow on inclined surfaces, *Numer. Heat Transfer* **2,** 497–509 (1979).
13. L. H. Thomas, The stability of plane Poiseuille flow, *Phys. Rev.* **91,** 780–783 (1953).
14. D. E. Müller, A method for solving algebraic equations using an automatic computer. *Mathl Tabl. Natn. Res. Coun., Wash.* **10,** 208–215 (1956).
15. G. B. Schubauer and H. K. Skramstad, Laminar boundary-layer oscillations and transition on a flat plate, *J. Res. Natn. Bur. Stand. (U.S.A.)* **38,** 251–292 (1947); see also *NACA Tech. Rep.* 909 (1948).
16. J. A. Ross, G. H. Barnes, J. G. Burns and M. A. S. Ross, The flat plate boundary layer. Part 3. Comparison of theory with experiment, *J. Fluid Mech.* **43,** 819–832 (1970).

CARACTERISTIQUES D'INSTABILITE D'ONDE POUR LE REGIME COMPLET DE CONVECTION MIXTE LE LONG DE PLAQUES PLANES VERTICALES

Résumé—L'instabilité ondulatoire de convection mixte le long d'un plan vertical est analysée par la théorie linéaire, pour le régime complet de convection mixte ($0 \leqslant \chi \leqslant 1$, $\chi = [1 + (Gr_x/Re_x^2)^{1/4}]^{-1}$) pour des fluides avec des nombres de Prandtl 0,7 et 7. Dans cette analyse, le domaine au delà de la frontière de la couche limite ($\eta \geqslant \eta_\infty$) est résolu analytiquement pour fournir les conditions aux limites à $\eta = \eta_\infty$. Ce traitement est important pour utiliser la transformations modifiée de Thomas lorsque λ est petit ($\lambda = Re_x^{1/2} + Gr_x^{1/4}$). Des solutions duales des valeurs critiques λ^* sont existantes dans le domaine $0 \leqslant \chi \leqslant 0{,}5$. Les résultats montrent que les deux courbes de stabilité neutre, l'une pour l'écoulement de Blasius ($\chi = 1$ ou $Gr_x = 0$, avec $\lambda^* = 290{,}6$) et l'autre pour l'écoulement pur de convection naturelle ($\chi = 0$ ou $Re_x = 0$, avec $\lambda^* = 33{,}33$) correspondant à deux modes différents.

EIGENSCHAFTEN DER WELLENINSTABILITÄT FÜR DEN GESAMTBEREICH DER GEMISCHTEN KONVEKTIONSSTRÖMUNG ENTLANG EINER VERTIKALEN EBENEN PLATTE

Zusammenfassung—Die Welleninstabilität der gemischten Konvektionsströmung entlang einer isothermen vertikalen ebenen Platte wird mit der linearen Theorie im Gesamtbereich der gemischten Konvektion ($0 \leqslant \chi \leqslant 1$, $\chi = [1 + (Gr_x/Re_x^2)^{1/4}]^{-1}$) für Fluide mit Prandtl-Zahlen zwischen 0,7 und 7 untersucht. Der Bereich über der Hauptströmungs-Grenzschichtkante ($\eta \geqslant \eta_\infty$) wird analytisch gelöst, um Grenzschichtbedingungen bei $\eta = \eta_\infty$ anstatt solchen bei $\eta = \infty$ zu beschaffen. Dieses Vorgehen ist wichtig bei der modifizierten Thomas-Transformation, wenn λ ($\lambda = Re_x^{1/2} + Gr_x^{1/4}$) klein ist. Zweifache Lösungen von kritischen Werten für λ^* treten in dem Bereich $0 \leqslant \chi \leqslant 0{,}5$ auf. Die Ergebnisse zeigen, daß die zwei begrenzenden neutralen Stabilitätskurven, die eine für die Blasius-Strömung ($\chi = 1$ oder $Gr_x = 0$, mit $\lambda^* = 290{,}6$) und die andere für die reine freie Konvektionsströmung ($\chi = 0$ oder $Re_x = 0$, mit $\lambda^* = 33{,}33$) zwei verschiedenen Erscheinungsformen entsprechen.

ХАРАКТЕРИСТИКИ ВОЛНОВОЙ НЕУСТОЙЧИВОСТИ РЕЖИМА СМЕШАННОЙ КОНВЕКЦИИ ОКОЛО ВЕРТИКАЛЬНЫХ ПЛОСКИХ ПЛАСТИН

Аннотация—Проводится анализ волновой неустойчивости течения при смешанной конвекции около изотермической вертикальной плоской пластины в рамках линейной теории для всего режима смешанной конвекции ($0 \leqslant \chi \leqslant 1$, $\chi = [1 + (Gr_x/Re_x^2)^{1/4}]^{-1}$) жидкостей с числами Прандтля, равными 0,7 и 7. Получено аналитическое решение для области основного течения вне пограничного слоя ($\eta \geqslant \eta_\infty$) при граничных условиях для $\eta = \eta_\infty$ вместо $\eta = \infty$. Такой подход эффективен при использовании модифицированного преобразования Томаса при малом λ ($\lambda = Re_x^{1/2} + Gr_x^{1/4}$). Найдено, что существуют неединственные решения для критических значений λ^* в диапазоне $0 \leqslant \chi \leqslant 0{,}5$. Полученные результаты показывают, что обе кривые предельной нейтральной устойчивости, одна из которых описывает течение Блазиуса ($\chi = 1$ или $Gr_x = 0$ при $\lambda^* = 290{,}6$), а другая только свободно-конвективное течение ($\chi = 0$ или $Re_x = 0$ при $\lambda^* = 33{,}33$), соответствуют различным модам течения.